Environmental Science
Water Research & Technology

ROYAL SOCIETY OF CHEMISTRY

PAPER

View Article Online
View Journal | View Issue

Cite this: *Environ. Sci.: Water Res. Technol.*, 2021, **7**, 2106

Precipitation-induced transport and phase partitioning of organophosphate esters (OPEs) in urban and rural watersheds†

Boluwatife Awonaike, Ying Duan Lei and Frank Wania *

Received 12th May 2021,
Accepted 20th September 2021

DOI: 10.1039/d1ew00329a

rsc.li/es-water

Organophosphate esters (OPEs) are extensively used as additives in industrial and consumer products as flame retardants, lubricants, and plasticizers. Such widespread occurrence coupled with precipitation-generated runoff can result in their transport from the atmosphere and terrestrial surfaces into water bodies. Using streamflow samples collected at high temporal resolution from two rivers in the Greater Toronto Area, Canada, we assessed the occurrence, distribution, transport, and likely sources of nine OPEs, covering a wide hydrophobicity range. Chlorinated OPEs (tris(2-chloroethyl) phosphate (TCEP), tris(1-chloro-2-propyl) phosphate (TCIPP) and tris(1,3-dichloro-2-propyl) phosphate (TDCPP)) were prevalent, making up 61% and 68% of total OPEs in the urban and rural rivers, respectively. OPE enrichment at high flow was observed at the outlet of the urban river, primarily due to precipitation-induced transport of particle bound OPEs. OPEs in the low $\log K_{OW}$ range like triethyl phosphate (TEP) and TCEP dominated the dissolved phase, while high $\log K_{OW}$ compounds like triphenyl phosphate (TPHP) and tris(2-ethylhexyl) phosphate (TEHP) were mostly adsorbed to particles. For OPEs that were sufficiently detected in both phases, calculated organic carbon–water distribution constants (K'_{OC}) were found to mostly be higher than values predicted using poly-parameter linear free energy relationships (ppLFERs), the open structure–activity/property relationship application (OPERA) and KOCWIN. Predictions made using EPISuite's molecular connectivity index (MCI) method and COSMOtherm were found to be closer to measured values. Particle bound OPEs can (i) sometimes occur at proportions higher than expected based on predicted equilibrium behavior and (ii) be major determinants of OPE occurrence and transport in urban aquatic environments during storm run-off.

Water impact

In addition to wet atmospheric deposition, storm-induced particle transport can greatly influence the enrichment of hydrophilic chlorinated OPEs in urban rivers. Empirically calibrated prediction tools may also have limitations which affect the accuracy of predicted organic carbon–water distribution constants (K_{OC}) for OPEs.

1 Introduction

Following the phase out of polybrominated diphenyl ethers (PBDEs), halogenated organophosphate esters (OPEs) have increasingly been used to meet the requirement of flame retardancy in industrial and consumer products. Non-halogenated OPEs are mostly used as plasticizers.[1] OPEs have also found uses in lubricants, glues, coatings, hydraulic fluids, textiles and lacquers.[2] Some OPEs have been found to have toxic and carcinogenic effects[1–4] leading to restrictions on their use. In Canada, tris(1-chloro-2-propyl) phosphate (TCIPP) and tris(1,3-dichloro-2-propyl) phosphate (TDCPP) are not permitted for use as food additives or in food-packaging materials, and tris(2,3-dibromopropyl) phosphate (TBPP) and tris(2-chloroethyl) phosphate (TCEP) have been banned from children's products.[5,6] Some states in the USA also have restrictions on the use of TCEP and TDCPP in residential furniture and children's products.[7] In Europe, TCEP has been phased out since the mid 1990s.[8] Nevertheless, these OPEs are still pervasive in environmental matrices, having been detected in precipitation,[9] surface water,[10] drinking water,[11] soil,[12] house dust,[13] wastewater effluent,[1] indoor and outdoor air,[14] biota, human milk,[15] and foodstuffs.[16,17] Being mixed in as additives and not chemically bonded to the matrix[18] increases the likelihood of OPEs migrating into the

Department of Physical and Environmental Sciences, University of Toronto Scarborough, 1265 Military Trail, Ontario, M1C 1A4, Canada.
E-mail: frank.wania@utoronto.ca

† Electronic supplementary information (ESI) available. See DOI: 10.1039/d1ew00329a

environment during production, use and disposal, making them readily available for uptake and transport.

The mobility of contaminants in the environment is enhanced during precipitation events. Rain and snow are effective scavengers of organic contaminants and can serve as entry pathways for OPEs into the aquatic environment.[9,19] Atmospheric deposition has been implicated as a source of OPEs to surface water; especially in urban areas, reflecting higher atmospheric concentration due to increased emissions from industries and the denser population in urban areas.[8,20,21] Estimations using a multimedia model suggested that OPE stream concentrations in Toronto, Canada were a result of wash-out of atmospheric emissions.[22] The observation of elevated OPE concentrations in Toronto urban air further highlights the importance of precipitation and washout as pathways for OPE transport.[23,24]

To build upon the existing knowledge of OPE transport in aquatic environments, we investigated the phase distribution of OPEs in two rivers in Toronto, and how this influences enrichment during wet weather. The two rivers have watersheds draining contrasting landscapes, and we explored the similarities and differences in occurrence and transport pathways of OPEs in both watersheds, as well as likely sources. We also present field-based organic carbon–water partitioning constants and compare these with other measured and predicted values. We found only one other study which investigated OPE distribution between suspended solids and water during rain events.[25] This work thus provides relevant insight into the fate, transport, and behavior of OPEs during precipitation in urban and rural aquatic environments.

2 Methods

The sample collection and extraction processes employed here are similar to those used for other organic contaminants in the context of a larger study on contaminant transport in aquatic environments.[26] These are summarized below.

2.1 Sampling

Baseflow and stormflow samples were collected at a headwater (HW) drainage point, around the middle (MD), and near the outlet (OL) of the Mimico Creek ("Mimico") and Little Rouge Creek ("Rouge") watersheds located in the Greater Toronto Area (GTA), Ontario, Canada (Fig. 1). Mimico, on the west side of the city, is one of the most urbanized watersheds in the GTA. It drains an area of about 68 km^2 and comprises part of Canada's busiest airport, Toronto Pearson International Airport, as well as roads, highways, golf courses, and industrial and residential areas. Rouge, on the eastern edge of Toronto, has a less developed watershed of 111 km^2 which is covered mostly by agricultural land (70%) and some suburban development in the south. Both drain into Lake Ontario and receive no direct input of effluent from wastewater treatment plants.

Automated samplers (Teledyne ISCO, Lincoln, Nebraska) were set up at each site and programmed to collect 1–2 L of water samples at 3-hour intervals on Aug. 21, 2018 (precipitation (P) = 25.6 mm at Mimico over approximately 13 h, 38.4 mm at Rouge over approximately 8 h, Average temperature (T_{avg}) = 21.8–22.8 °C, 50 mm of rainfall in preceding two weeks). Samples were collected into glass bottles that had been pre-combusted for 8 h at 450 °C. Additional grab samples were collected at 24-hour intervals following the event (using a polyethylene bottle attached to a sampling rod) until flow receded to baseflow conditions. In total, about 11–16 discrete samples were collected at each site. Rainwater was also collected at each site into pre-cleaned 2.5 L amber jars fitted with a 32 cm diameter galvanized steel funnel. Rainwater samples at MMD could not be obtained due to a sampling error. Stream discharge (Q) was calculated from stage-discharge rating curves established at each site using area–velocity based discharge measurements calibrated to continuous, digital measurement of stage using pressure transducers.

Samples were immediately transferred to the laboratory, stored at 4 °C and passed through pre-combusted glass fiber

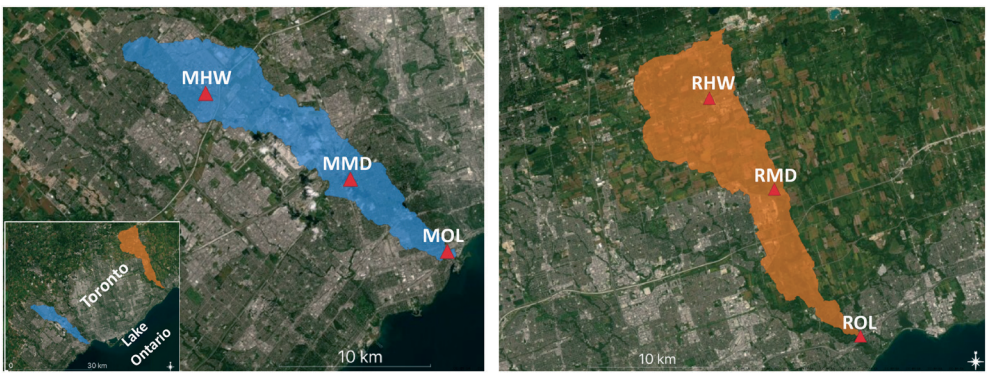

Fig. 1 Mimico (blue) and Little Rouge Creek (orange) watersheds, showing sampling locations at the headwater (HW), middle (MD) and outlet (OL), denoted as MHW, MMD, MOL in Mimico, and RHW, RMD, ROL in Rouge. Maps generated using QGIS; basemap: ESRI; map data: Ontario Ministry of Natural Resources and Forestry. Reprinted (adapted) with permission from Awonaike *et al.* (2021).[26] Copyright 2021 American Chemical Society.

filters (GFFs, Whatman, Brentford, UK; 0.7 μm) within three weeks to isolate dissolved and particulate fractions. The "dissolved phase" here comprises anything that was able to pass through the filter and is not corrected for the likely presence of colloids to which contaminants may sorb. Filtrates and filters containing particles were stored at 4 and −20 °C respectively until extraction. Subsamples of about 300 mL were also passed through dry, pre-weighed GFFs to determine the suspended solids (SS) concentration from the increase in mass upon drying to a constant weight. Particulate organic carbon (POC) analysis with a Flash 2000 organic elemental analyzer (Thermo Scientific, USA) was achieved by gently scraping SS (when possible) from the surface of the filter into precleaned amber vials.

2.2 Sample extraction and quantification

The nine OPEs considered in this study are trimethyl phosphate (TMP), triethyl phosphate (TEP), tripropyl phosphate (TPrP), tri(*n*-butyl) phosphate (TNBP), tris(2-chloroethyl) phosphate (TCEP), tris(1-chloro-2-propyl) phosphate (TCIPP), tris(1,3-dichloro-2-propyl) phosphate (TDCPP), triphenyl phosphate (TPP) and tris(2-ethylhexyl) phosphate (TEHP) (Table S1†). These were extracted from the dissolved phase by solid phase extraction (SPE) using Oasis HLB cartridges (500 mg, 6 mL, Waters, Canada) and 12 mL of dichloromethane (DCM) as the elution solvent. Samples were spiked with 80 ng of surrogate standards (TEP-d_{15}, TNBP-d_{27}, TCEP-d_{12} and TPHP-d_{15}), before being passed through cartridges pre-conditioned with 2 mL methanol, 3 mL DCM, 3 mL methanol and 2 mL de-ionized water. The vessel containing the water sample during SPE was also rinsed with 33 mL DCM to collect any compounds sorbed to the vessel wall. Samples which showed ice formation upon freezing were dried by passing them through a column of sodium sulphate.

Particles on the GFFs underwent accelerated solvent extraction (ASE) (Dionex Corp, California, USA) with 50 : 50 hexane : acetone using the following conditions: 75 °C, 1500 psi, 5 min static time, 3 static cycles, 100% flush volume, and 240 s of purging.[27] Both dissolved and suspended solid phase extracts were concentrated under a gentle stream of N_2 and solvent exchanged into isooctane. 100 ng of mirex was added to each sample as an injection standard before analysis. OPEs in extracts were quantified using an Agilent 7890A gas chromatograph coupled to an Agilent 7000A triple quadrupole mass spectrometer in electron impact ionization mode (full details in Text S1†). OPE concentrations in water samples were determined from a plot of the ratio of the analyte to injection standard response as a function of analyte concentration in the calibration standards.

For QA/QC, we included lab and field blanks, labelled surrogate spikes and occasional duplication. Lab blanks comprised of surrogate spiked de-ionized water (SPE), and surrogate spiked pre-baked GFFs (ASE) for every batch of 6–8 samples. Field blanks were generated by exposing de-ionized water and clean GFFs for one minute at the sampling sites. Recoveries of the TEP-d_{15}, TNBP-d_{27}, TCEP-d_{12} and TPHP-d_{15} were 76%, 88%, 98% and 86% respectively for SPE and 75%, 79%, 91% and 99% for ASE (more details in Table S2†). TEP-d_{15} had the lowest recoveries in both extractions and given its relatively high volatility, this is a likely result of loss during N_2 blowdown. SPE blanks were more contaminated than ASE blanks, especially with TNBP, chlorinated OPEs and TPP (Table S2†) likely as a result of sample contact with plastics (*e.g.*, SPE cartridges, PTFE transfer tubes) during the extraction process.[28,29] All samples were blank and recovery-corrected to account for these effects. Due to the loss of four particle phase peak flow samples at MMD during the analysis, reported values for OPEs in the particle phase and total OPEs at this site are likely underestimated.

2.3 Calculations

Event average concentrations in units of ng L^{-1} were calculated for each storm on a time-weighted basis using:

$$[\mathrm{OPE}]_{\mathrm{TWA}} = \frac{\sum_{i}^{n} (C_i \Delta t_i)}{\sum_{i}^{n} (\Delta t_i)}$$

Flow-weighted average concentrations, calculated for comparison, are presented in Fig. S1,† and were calculated using:

$$[\mathrm{OPE}]_{\mathrm{FWA}} = \frac{\sum_{i}^{n} (C_i Q_i \Delta t_i)}{\sum_{i}^{n} (Q_i \Delta t_i)}$$

OPEs storm loads at each site were calculated using:

$$\mathrm{Load} = \sum_{i}^{n} (C_i Q_i \Delta t_i)$$

where i and n represent the first to last samples for a given storm, C_i is the concentration of the ith sample, Q_i is the stream discharge at the time of the ith sample, and Δt_i is the time interval over which C_i and Q_i are considered to apply.

For the calculation of averages and loads, values below the detection limit were substituted with half of the detection limit for each compound.[30]

Field-based distribution constants between suspended solid organic carbon and water (K'_{OC}) were calculated thus:

$$K'_{\mathrm{OC}} = \frac{C_{\mathrm{PP}}}{C_{\mathrm{DP}}} \times \frac{1}{f_{\mathrm{OC}}}$$

where C_{PP} and C_{DP} are the concentrations in the particle phase (ng kg^{-1}) and the dissolved phase (ng L^{-1}) respectively, and f_{OC} is the fraction of organic carbon in particles.

2.4 Prediction of K_{OC}

For comparison with distribution constants between organic carbon and the aqueous phase (K'_{OC}) derived from the measured concentrations, we predicted the equilibrium partitioning constants at a temperature of 25 °C for the nine OPE using five different techniques. This included the K_{OW} method and Sabljic's molecular connectivity index (MCI) method as implemented in KOCWIN™ in the US EPA's Estimation Program Interface Suite (EPISuite)[31] and the log K_{OC} function of the open structure–activity/property relationship application (OPERA, version 2.6).[32]

The third method involved the use of polyparameter linear free energy relationships (ppLFERs) as implemented in the UFZ LSER database.[33] ppLFERs capture all types of molecular interactions that are relevant for the phase transfer of neutral organic chemicals, and for K_{OC}, take the general form of:[34]

$$\log K_{OC} = c + eE + sS + aA + bB + vV$$

The upper-case letters are the solute descriptors and describe the following solute properties: E, excess molar refraction; S, dipolarity/polarizability parameter; A, solute H-bond acidity; B, solute H-bond basicity; V, McGowan's molar volume with units of (cm^3 mol^{-1})/100; and L, the logarithmic hexadecane–air partition constant. The coefficients e, s, a, b, and v are parameters that depend on the difference in chemical properties between water and the suspended solid organic matter phase.[34]

Two K_{OC} ppLFERs available in the UFZ database were used for our estimations.[34,35] Experimentally determined solute descriptors from the database were used in the ppLFERs for all target OPEs except TCIPP and TEHP, for which we predicted these descriptors by inputting simplified molecular-input line-entry system (SMILES) into quantitative structure property relationships (QSPRs) available in the UFZ-LSER database.

Finally, K_{OC} was predicted using COSMOtherm, which calculates solvation mixture thermodynamics based on quantum chemistry using COSMO-RS theory.[36,37] SMILES strings for the OPEs were converted to spatial data files (.sdf) using Open Babel.[38] These .sdf files served as input data for optimized TURBOMOLE (v. 4.1.1, COSMOlogic GmbH & Co. KG, Leverkusen, Germany, 2017) calculations, which generates COSMOfiles. COSMOfiles were generated for the OPEs and representative organic matter molecules. Atalay *et al.*[39] describes 16 hypothetical molecular structures to represent organic matter (OM), broadly divided into three groups of soil humic acids (HA), aquatic HA and aquatic fulvic acids (FA). Phillips *et al.*[40] also describe a method for using these model organic matter molecules to predict K_{OC} using a quantum chemical modeling technique. For the calculations done here, only seven OM molecules consisting of three aquatic HA and four aquatic FA were used. The generated COSMOfiles were fed into the COSMOtherm software (version C30_1705, COSMOlogic GmbH & Co. KG, Leverkusen, Germany, 2017) to calculate $\log K_{OC}$ using the $\log P$/$\log D$ function. The average of the seven $\log K_{OC}$ values are presented below. $\log K_{OC}$ values for individual molecules can be found in Table S3 in the ESI.†

3 Results and discussion

3.1 OPEs in urban and rural watersheds – occurrence, sources and storm-induced transport

Of all the target OPEs, chlorinated OPEs were detected at the highest concentrations in all samples, making up 61% and 68% of total OPEs in Mimico and Rouge, respectively (Table 1). TMP and TPP, on the other hand, were scarcely detected in any of the samples. As Hao *et al.* (2018)[41] neither detected TPP in the Toronto area, its absence is likely a result of it not being used in this region. In the case of TMP, infrequent detections could be a result of low retention by the Oasis HLB cartridge due to its high polarity and volatility.[42] TEP-d_{15}, which is closest in structure to TMP, indeed had the lowest recoveries in both dissolved and particle phase extractions. All dissolved and particle phase concentrations can be found in Tables S3 and S4.†

The range of the OPE concentrations in Mimico and Rouge are compared with those reported by other studies in Table 1. TCIPP had the highest concentrations in Mimico and Rouge, similar to observations in rivers in Germany, Austria and Netherlands (Table 1). In the more urbanized Mimico Creek, total OPE concentrations were lower than in another urban stream in Toronto – plausibly due to factors including differing emission strengths or wastewater input (the exact location and external inputs to this stream is unknown), but comparable to those in European rivers influenced by wastewater and other anthropogenic activities.[43,44] However, even in Rouge, levels were higher than in the Great Lakes, including Lake Ontario, into which it drains.[45]

Time-weighted average concentrations of OPEs in the dissolved phase ranged from 138 to 275 ng L^{-1} at Mimico, and from 48 to 75 ng L^{-1} at Rouge (Fig. 2a). Particle phase concentrations were an order of magnitude lower with a range of 11 to 46 ng L^{-1} at Mimico and 4 to 5 ng L^{-1} at Rouge (Fig. 2b). Flow-weighted average concentrations, which are known to sometimes deviate from time-weighted averages, especially in cases where concentrations are heavily influenced by streamflow, were similar to time-weighted averages for dissolved OPEs (140 to 317 ng L^{-1} at Mimico, 59 to 113 ng L^{-1} at Rouge), but much higher for particle OPEs at Mimico, especially MOL (Fig. S1†). In both rivers, all OPEs except TEHP were 67 to 98% present in the dissolved phase. TEHP, instead favoured the particle phase, unsurprising, given its high $\log K_{OC}$. When normalized by sub watershed area, dissolved phase loads ranged from 0.3 to 2.1 g km^{-2} at Mimico, and 0.4 to 1.4 g km^{-2} at Rouge (Fig. 2a). The differences between both watersheds are less pronounced when expressed as loads, reflecting similar dissolved phase

Table 1 Measured OPE concentrations (ng L^{-1}) in various locations around the world

Location	TEP	TCEP	TCIPP	TDCPP	TNBP	TPHP	Ref.
Mimico Creek, Toronto	30–72	39–73	27–116	3–24	10–25	6–18	
Little Rouge Creek, Toronto	8–17	3–21	23–26	3–12	1–2	2–8	
Urban stream, Toronto	70	100–190	290–2010	130	140–1230	ND	41
Five Great Lakes[b]	NA	0.1–2	0.4–17	0.2–7	0.1–5	0.1–3	45
Elbe river, Germany[a,b]	7–34	5–20	40–250	6–31	2–8	0.3–4	43
Rhine Delta, Netherlands[a,b]	30–83	12–25	75–160	13–31	6–28	1–2	43
Surface water, Austria[a]	13–51	13–130	33–170	7–19	20–110	6–10	44
Ruhr river, Germany[a]	NA	13–130	20–200	50	30–110	40	1
Swedish rivers[a]	NA	0.7–7	5–30	0.1–48[c]	3–24	NA	46
Songhua river, China[a,b]	5–190	38–3700	5–190	2–46	87–960	5–65	42

[a] Wastewater or anthropogenically impacted sites. [b] Dissolved phase concentrations only. [c] Sum of TDCPP and TEHP concentrations. NA: not analyzed, ND: not detected.

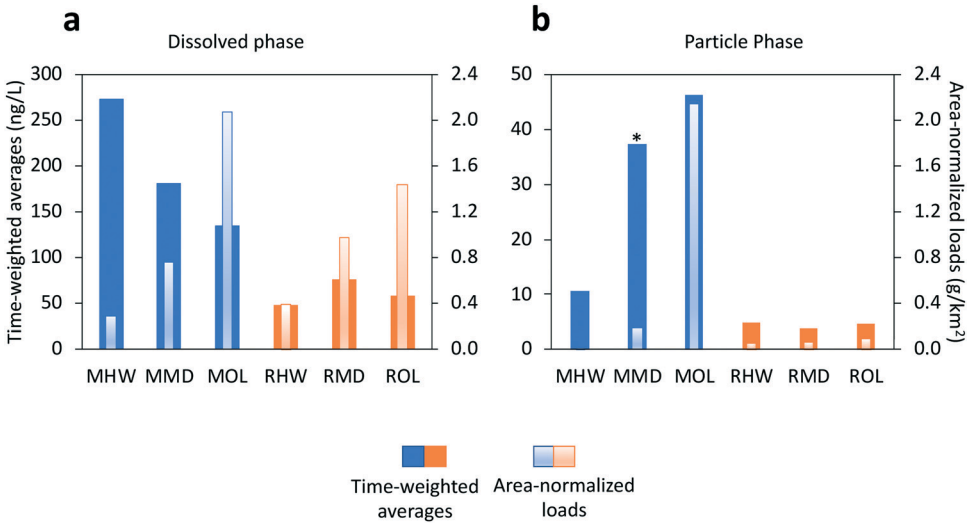

Fig. 2 Time weighted averages and area-normalized loads of OPEs in the (a) dissolved phase and (b) particle phase. *MMD values are underestimated due to missing peak flow samples.

OPE transport in both watersheds. Particle phase area-normalized loads (Fig. 2b) ranged from 0.01 to 2.14 g km^{-2} at Mimico, and 0.05 to 0.1 g km^{-2} at Rouge, indicating the more predominant OPE-contaminated particle transport in the Mimico watershed during the rain event. Particle bound OPEs made up 4 to 51% of total loads at Mimico and only 6 to 11% at Rouge. Total OPEs loads in the urban river were 3 to 10 times higher than at the rural location.

Higher OPE concentrations in urban *vs.* rural rivers have been reported in Germany[8] and China.[47] Higher urban OPE concentrations have also been reported in outdoor dust[48] and human hair.[49] Increased OPE emissions are associated with urban areas due to higher human activity and population density.[46] Mimico Creek watershed contains a large network of roads and busy highways, and traffic has been shown to be a source of OPEs *via* emissions from vehicle ventilation systems or leakage of motor oils and lubricants,[50] which can then be washed out of the atmosphere and washed off urban surfaces during precipitation. In addition, the airport located in the Mimico watershed is a plausible source of OPEs. A river close to an airport in Albany, New York was found to contain up to 25 000 ng L^{-1} of OPEs, resulting from the use of OPEs in aircraft hydraulic fluids and lubricants.[51] The build-up of OPEs in the atmosphere and on urban surfaces during periods of no precipitation creates non-point OPE sources to the creek during rainfall.

Chemographs showing how the stream water concentrations of the OPEs in the dissolved and particle phase changed during the run-off event are displayed in Fig. 3a and 4a, respectively. OPEs in the dissolved phase, which were dominated by TEP, TCEP and TCIPP, did not show a consistent enrichment or dilution trend in either creek (Fig. 3a). Dissolved OPEs increased with streamflow only at the Mimico headwater (MHW) and the Rouge outlet (ROL). MHW also had the highest concentration of dissolved OPEs in stormflow ($[\text{dissolved-OPE}]_{TWA}$ = 275 ng L^{-1}) (Fig. 3a) and rainwater (412 ng L^{-1}) (Fig. 3b). Other sites either showed a dilution of OPE in stream water during the event, or were chemostatic, with rainwater concentrations ranging

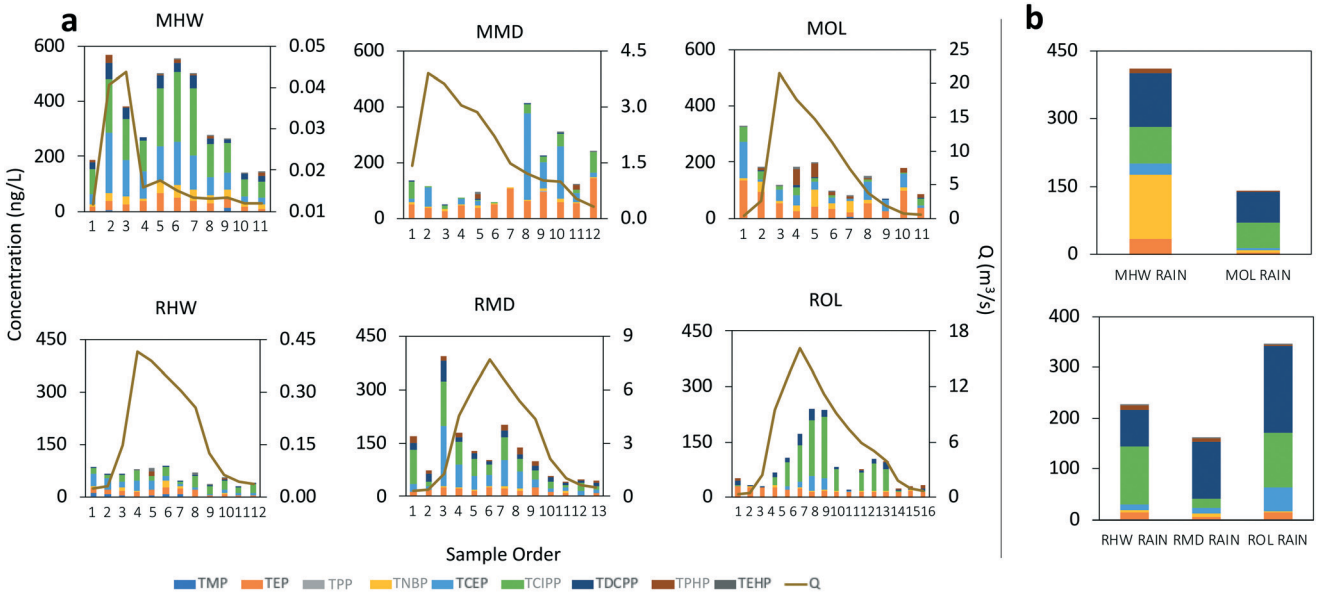

Fig. 3 OPE composition and concentration in dissolved phase samples from (a) stormflow and (b) rainwater in Mimico (top) and Rouge (bottom) watersheds. During the event, samples (1–8) were taken at 3-hour intervals, whereas the last few samples (9 and above) were taken at 24-hour intervals.

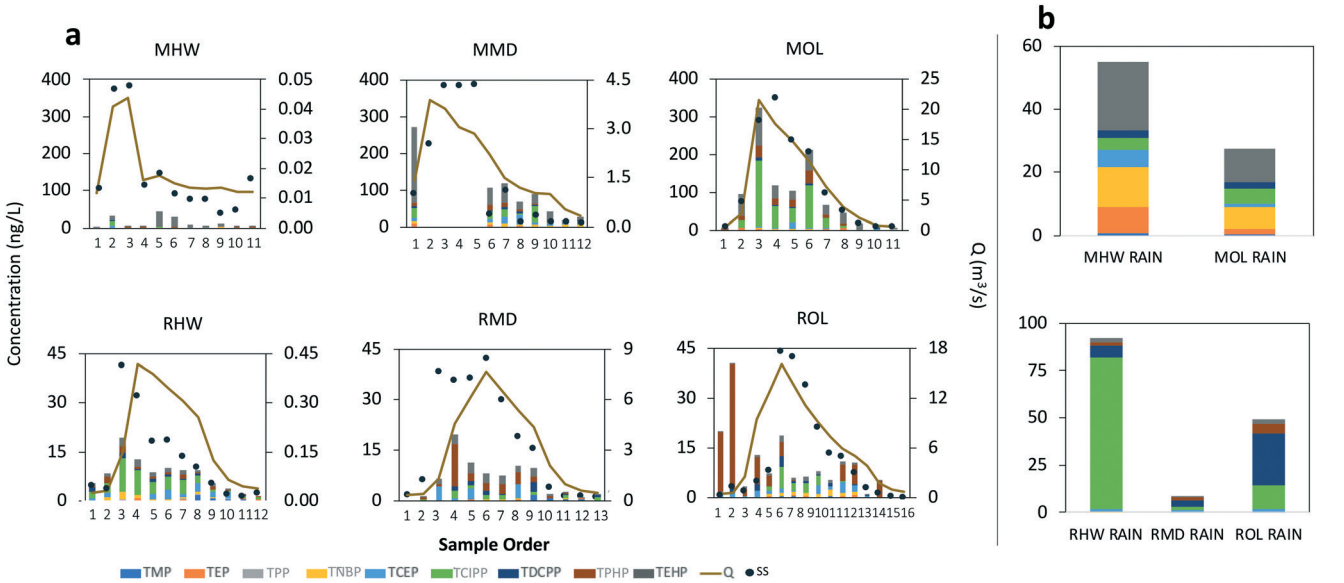

Fig. 4 OPE composition and concentration in particle phase samples from (a) stormflow and (b) rainwater in Mimico (top) and Rouge (bottom) watersheds. During the event, samples (1–8) were taken at 3-hour intervals, whereas the last few samples (9 and above) were taken at 24-hour intervals. Particle bound OPEs could not be quantified in MMD samples 2–5 due to sample loss.

from 139 to 345 ng L^{-1}. OPE composition in rainwater was largely similar at sites within a watershed, with the chlorinated OPEs being predominant (Fig. 3b and 4b).

The higher OPE concentrations in rain and in the dissolved phase of stormwater at MHW is consistent with the area around MHW generally being more industrialized than MMD, MOL and the Rouge sites. In particular, the high TNBP concentration in the rain sample collected at MHW (Fig. 3b) is not seen at other sites. TNBP is imported into Canada for use as a flame retardant in aviation hydraulic fluids[52] and of all the rain samples collected, those from MHW were closest to the vicinity of the airport. Similarly, TNBP was dominant in snow samples collected from an airport in Sweden.[50] However, it was not found to be dominant in river samples collected near an airport in Albany, New York, suggesting that the specific OPEs used in aviation hydraulic fluids vary spatially (TNBP was also not dominant in hydraulic fluids analyzed in the same study).[51]

OPEs in the suspended particle phase were dominated by TCIPP, TPHP and TEHP (Fig. 4a). TPHP and TEHP have log K_{OW} values >4 and are expected to be predominantly sorbed to particles as is observed here. With a log K_{OW} of 2.59,[2] TCIPP may be expected to show negligible partitioning to the particles, and while this was the case at five of the sites, 64% of it was particle-bound at MOL. This indicates the presence of particles highly contaminated with TCIPP at this outlet location. MOL also had the highest concentration of all particle phase OPEs and showed a clear enrichment with increasing stormflow during the event (the trend and concentrations at MMD cannot be ascertained due to missing peak flow samples, Fig. 4a). While particle bound OPE concentrations in rain (Fig. 4b) were higher at MHW than at MOL, this is not the case in stormflow samples, suggesting the presence of sources of OPE-contaminated particles at MOL, other than wet deposition. Although no OPEs were found in plastic debris and pre-production pellets collected from the Mimico watershed area (data not shown), TCIPP, TPHP and TEHP are used in other consumer products including upholstered furniture, mattresses, glues, textile waterproofing spray and electronic equipment. They have also found use in building and construction materials, paints and coatings, as well as in motor oil and hydraulic fluids.[2] The city of Toronto, where MMD and MOL are located also has two times the population density, and thus increased human activity, of the city of Brampton, where MHW is located.[53] Increased population and human activity have been implicated as sources of OPEs in rivers with[46] and without[21] nearby manufacturing plants or WWTPs. The different OPE composition in the particle phase of rainwater samples between Mimico and Rouge (Fig. 4b) is another indicator of differences in use and emissions between urban and rural areas. In rainwater samples from Rouge, TCIPP and TDCPP are dominant, but in Mimico, there is more of TNBP and TEHP – which are widely used in industrial processes.[2]

Most earlier studies quantified OPEs only in the dissolved phase (Table 1), because the relatively high water solubility of these compounds may indicate a limited role for the suspended particle phase. Our results demonstrate that enhanced partitioning of some OPEs to the particle phase is possible, notwithstanding their presumed equilibrium partitioning properties (discussed further below). Disregarding the particle phase may result in underestimated OPE concentrations, especially for TCIPP, in rain and stream water. During the run-off event, we observed that the transport and enrichment of OPEs at some locations was in fact governed more by the particle bound fraction than by freely dissolved OPEs. Müller *et al.*[25] also observed high particle-associated input of TCIPP in a German river over the course of a rainfall. They found that although dissolved phase OPE concentrations were higher, the mass loads in the particle phase were comparable or sometimes higher than in the dissolved phase, which is similar to our observations here.

3.2 Distribution of OPEs between organic carbon and water

For the five OPEs (TCEP, TCIPP, TNBP, TDCPP and TPHP) that were detected in both phases in at least one sample, we calculated the field-based logarithm of the partitioning constants between suspended solid organic carbon and water (log K'_{OC}). TCIPP (n = 31) and TPHP (n = 19) were most and least frequently detected in both dissolved and particle phase. Average log K'_{OC} values from all sites were compared with values of log K_{OC} predicted using different methods (Fig. 5).

There are remarkable differences between the predicted and the field observed log K_{OC} values. Whereas all prediction methods agree that the log K_{OC} should vary between the OPEs – with lower values for TCEP and TCIPP and higher values for TDCPP and TPHP, such a trend is not apparent in the field-derived values, where values only fall within a narrow range of 4.0 to 4.5. This is mostly because the predicted log K_{OC} for the smaller, less hydrophobic OPEs (especially TCEP and TCIPP) are generally lower than the ones observed in the field, whereas predicted and measured values are in better agreement for the larger OPEs (*e.g.*, TPHP). Higher than expected log K'_{OC} values for TCEP, TCIPP and TNBP have been observed in other field studies.[54,55] This has also been observed for TCIPP in measured values of log K_D (sediment-water partitioning constant),[25] and for TCEP and TCIPP in measured values of log K_{DOC} (dissolved organic carbon-water partitioning constant).[56]

The least agreement with measured values was observed with the OPERA model (root mean square errors (RMSE) = 1.9). The ppLFERs and the EPISuite K_{OW} method also agreed poorly with measured values (RMSE from 1.5 to 1.8). The above prediction methods were all commonly calibrated with empirical training sets, some of which do not include organic phosphates, which is likely the reason for the poor correlations observed. Although the OPERA model indicates that all five OPEs fall within the applicability domain of the model, the local applicability domain index only falls between 0.47 and 0.59 for these compounds, indicating that the predictions should be considered with caution.[32]

The log K_{OC} values predicted by COSMOtherm, a non-empirical quantum chemical based modeling tool, and the MCI method, a semiempirical model[57] are generally higher than those predicted by the other techniques and in better agreement with the observations (RMSE = 0.9 and 0.8 respectively). Interestingly, while the COSMOtherm and MCI predictions are in good agreement with each other for the chlorinated OPEs (TCEP, TCIPP and TDCPP), this is not the case with TNBP and TPHP. It is possible that the semi-empirical nature of the MCI model interferes with its ability to properly predict log K_{OC} for certain polar compounds. This could be because the training set for the empirical portion of the MCI model includes chlorfenvinphos, an organic compound with contains the phosphate group and additional chlorine atoms, similar to TCEP, TCIPP and TDCPP. There are, however, no tri-alkyl or tri-aryl phosphates in this

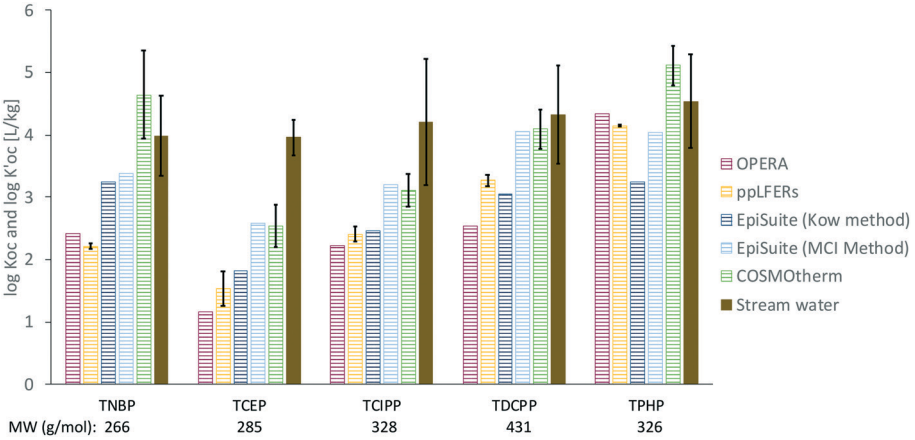

Fig. 5 Values of measured $\log K'_{OC}$ and predicted $\log K_{OC}$ for OPEs. Values shown for ppLFERs, COSMOtherm and stream water are averages. Error bars show the range of two values for ppLFERs and standard deviations for COSMOtherm and measured values. Individual measurements and predictions can be found in Table S3.† The approximate molecular weight (MW) of each OPE is also shown.

training set.[57] Also, COSMOtherm-generated σ-profiles, which depict the probability distribution of a molecular surface segment that has a specific charge density (σ),[58] show that regardless of its relatively smaller molecular weight, TNBP is the least polar of these five OPEs, seen in the narrow distribution of σ around zero[37] (Fig. 6). This would account for the higher values observed (3.3 to 4.9) and predicted with COSMOtherm (3.4 to 5.8) (Table S3†). The empirical nature of the other models likely does not fully take this reduced polarity into account, leading to lower $\log K_{OC}$ predictions for TNBP. TCEP, TCIPP, TPHP and TDCPP generally showed similar, more polar σ-profiles.

Although the non-empirical COSMOtherm model predicts values in better agreement with measured values at individual sampling sites (Table S3†), we are unable to find an obvious reason why large discrepancies exist for TCEP and TCIPP. The probability ($p(\sigma)$) of having a non-polar surface segment *i.e.* $\sigma = 0$ (ref. 59) is almost identical for TCIPP, TPHP and TDCPP (Fig. 6). This means that these compounds have approximately the same amount of surface area available for non-polar interactions. While this may partially explain the higher and similar $\log K'_{OC}$ measured for TCIPP, TPHP and TDCPP, it does not explain the lack of a corresponding similarity in COSMOtherm predicted values (which were estimated using the same σ-profiles). It is important to note that the morphology of the organic matter can also influence these interactions. Some studies have attributed such discrepancies to time and location-specific differences in soil and organic carbon nature,[54,60] and organic carbon mineralization.[61] Additionally, field derived $\log K'_{OC}$ values may not accurately reflect equilibrium conditions, especially given the use of OPEs in everyday products which can easily be deposited in particulate form *e.g.*, foam. Further investigations are necessary to broaden our knowledge of the organic carbon–water partitioning of OPEs.

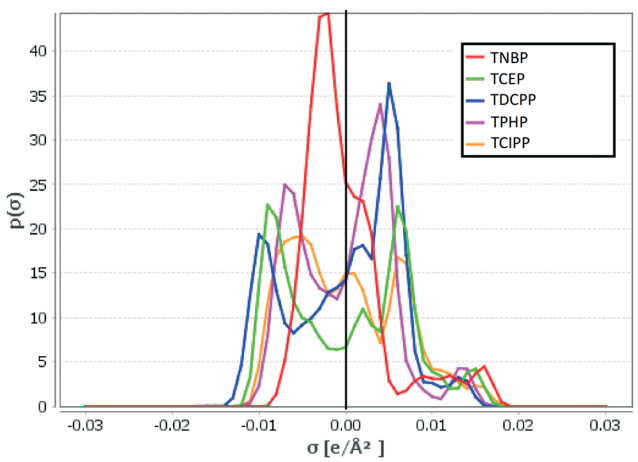

Fig. 6 σ-Profiles for OPEs showing screening charge density (σ) and probability distribution of molecular segments that have a specific value of σ. $\sigma = 0$ represents the non-polar surface segment, and polarity increases with increasing distance from 0 in either direction.[59] Plot generated using COSMOtherm (version C30_1705, COSMOlogic GmbH & Co. KG, Leverkusen, Germany, 2017).

4 Conclusion

Our study highlights the importance of the suspended solid phase in the fate and transport of OPEs in urban aquatic environments. OPEs in the urban watershed outlet were transported *via* suspended solids and led to an enrichment during the runoff event while dissolved OPEs were found not to become enriched. We also show that OPEs like TCIPP can exist in the particle phase in proportions much higher than expected based on predicted equilibrium behaviour. Measuring OPEs in the dissolved phase alone can thus lead to underestimations of actual environmental concentrations. Predictions of $\log K_{OC}$ using ppLFERs, OPERA and the EPISuite K_{OW} method were lower than field values. However, COSMOtherm predicted values were in better agreement with field values for all OPEs. Our study presents new and

complementary information on the transport behaviour, partitioning and property prediction of OPEs which will inform future investigations into this group of compounds in the environment.

Limitations of this study include the analysis of only 9 OPEs, especially given the constant uncovering of novel OPEs in the environment,[62,63] the loss of some samples at MMD, leading to the likely underestimation of average concentrations, and the uncertainty of field-based measurements of partitioning constants between organic carbon and water given that organic matter can occur in a variety of forms *e.g.*, soot, brown carbon, fly ash, which can influence the partitioning of organic compounds to this medium.

Conflicts of interest

There are no conflicts to declare.

Acknowledgements

We are grateful to Environment and Climate Change Canada for the loan of automated water samplers. We also acknowledge the help of Endo Satoshi in interpreting COSMOtherm data. Funding from the Natural Sciences and Engineering Research Council of Canada, TD Canada Trust (B. A.), an Ontario Graduate Scholarship (B. A.), a fellowship from Delta Kappa Gamma World International (B. A.) are further acknowledged.

References

1 J. A. Andresen, A. Grundmann and K. Bester, *Sci. Total Environ.*, 2004, **332**, 155–166.
2 I. van der Veen and J. de Boer, *Chemosphere*, 2012, **88**, 1119–1153.
3 J. G. Camarasa and E. Serra-Baldrich, *Contact Dermatitis*, 1992, **26**, 264–265.
4 J. Björklund, S. Isetun and U. Nilsson, *Rapid Commun. Mass Spectrom.*, 2004, **18**, 3079–3083.
5 Environment and Climate Change Canada, *Flame retardants*, https://www.canada.ca/en/health-canada/services/chemicals-product-safety/flame-retardants.html#s3, (accessed January 2021).
6 Environment and Climate Change Canada, *Updated Draft Screening Assessment Certain Organic Flame Retardants Substance Grouping*, https://www.canada.ca/content/dam/eccc/documents/pdf/pded/ofr-tcpp-tdcpp/Draft-screening-assessment-tcpp-tdcpp.pdf, (accessed January 2021).
7 *Safer States: Toxic Flame Retardants*, https://www.saferstates.org/toxic-chemicals/toxic-flame-retardants/, (accessed January 2021).
8 J. Regnery and W. Püttmann, *Water Res.*, 2010, **44**, 4097–4104.
9 J. Regnery and W. Püttmann, *Clean: Soil, Air, Water*, 2009, **37**, 334–342.
10 Y. Shi, L. Gao, W. Li, Y. Wang, J. Liu and Y. Cai, *Environ. Pollut.*, 2016, **209**, 1–10.
11 P. E. Stackelberg, J. Gibs, E. T. Furlong, M. T. Meyer, S. D. Zaugg and R. L. Lippincott, *Sci. Total Environ.*, 2007, **377**, 255–272.
12 E. Fries and I. Mihajlović, *J. Environ. Monit.*, 2011, **13**, 2692.
13 H. M. Stapleton, S. Klosterhaus, S. Eagle, J. Fuh, J. D. Meeker, A. Blum and T. F. Webster, *Environ. Sci. Technol.*, 2009, **43**, 7490–7495.
14 L. Zhou, M. Hiltscher, D. Gruber and W. Püttmann, *Environ. Sci. Pollut. Res.*, 2017, **24**, 10992–11005.
15 A. M. Sundkvist, U. Olofsson and P. Haglund, *J. Environ. Monit.*, 2010, **12**, 943–951.
16 J. Li, L. Zhao, R. J. Letcher, Y. Zhang, K. Jian, J. Zhang and G. Su, *Environ. Int.*, 2019, **127**, 35–51.
17 L. Zhao, K. Jian, H. Su, Y. Zhang, J. Li, R. J. Letcher and G. Su, *Environ. Int.*, 2019, **128**, 343–352.
18 A. K. Greaves and R. J. Letcher, *Bull. Environ. Contam. Toxicol.*, 2017, **98**, 2–7.
19 I. Mihajlović and E. Fries, *Atmos. Environ.*, 2012, **56**, 177–183.
20 U.-J. Kim and K. Kannan, *Environ. Sci. Technol.*, 2018, **52**, 5625–5633.
21 A. Bacaloni, F. Cucci, C. Guarino, M. Nazzari, R. Samperi and A. Laganà, *Environ. Sci. Technol.*, 2008, **42**, 1898–1903.
22 T. F. M. Rodgers, J. W. Truong, L. M. Jantunen, P. A. Helm and M. L. Diamond, *Environ. Sci. Technol.*, 2018, **52**, 12465–12474.
23 M. Shoeib, L. Ahrens, L. Jantunen and T. Harner, *Atmos. Environ.*, 2014, **99**, 140–147.
24 A. Saini, J. Clarke, N. Jariyasopit, C. Rauert, J. K. Schuster, S. Halappanavar, G. J. Evans, Y. Su and T. Harner, *Environ. Pollut.*, 2019, **247**, 89–97.
25 M. E. Müller, C. Zwiener and B. I. Escher, *Environ. Toxicol. Chem.*, 2021, **40**, 88–99.
26 B. Awonaike, Y. D. Lei, A. Parajulee, C. P. J. Mitchell and F. Wania, *ACS ES&T Water*, 2021, **1**, 1209–1219.
27 A. Parajulee, Y. D. Lei, A. Kananathalingam, D. S. McLagan, C. P. J. Mitchell and F. Wania, *Water Res.*, 2017, **124**, 407–414.
28 K. Liang, Y. Niu, Y. Yin and J. Liu, *J. Environ. Sci.*, 2015, **34**, 57–62.
29 S. H. Brandsma, J. de Boer, P. E. G. Leonards, W. P. Cofino, A. Covaci and P. E. G. Leonards, *TrAC, Trends Anal. Chem.*, 2013, **43**, 217–228.
30 R. A. Hites, *Environ. Sci. Technol.*, 2019, **53**, 11059–11060.
31 US EPA, *Estimation Programs Interface Suite™ for Microsoft® Windows, version 4.11*, 2021.
32 K. Mansouri, C. M. Grulke, R. S. Judson and A. J. Williams, *J. Cheminf.*, 2018, **10**, 10.
33 N. Ulrich, S. Endo, T. N. Brown, N. Watanabe, G. Bronner, M. H. Abraham and K.-U. Goss, *UFZ - LSER Database v 3.2.1*, 2017, http://www.ufz.de/lserd, (accessed February 2021).
34 T. H. Nguyen, K.-U. Goss and W. P. Ball, *Environ. Sci. Technol.*, 2005, **39**, 913–924.
35 S. K. Poole and C. F. Poole, *J. Chromatogr. A*, 1999, **845**, 381–400.
36 A. Klamt, *Wiley Interdiscip. Rev.: Comput. Mol. Sci.*, 2011, **1**, 699–709.

37 F. Eckert and A. Klamt, *AIChE J.*, 2002, **48**, 369–385.
38 N. M. O'Boyle, M. Banck, C. A. James, C. Morley, T. Vandermeersch and G. R. Hutchison, *J. Cheminf.*, 2011, **3**, 33.
39 Y. B. Atalay, R. F. Carbonaro and D. M. Di Toro, *Environ. Sci. Technol.*, 2009, **43**, 3626–3631.
40 K. L. Phillips, D. M. Di Toro and S. I. Sandler, *Environ. Sci. Technol.*, 2011, **45**, 1021–1027.
41 C. Hao, P. A. Helm, D. Morse and E. J. Reiner, *Chemosphere*, 2018, **191**, 288–295.
42 X.-W. Wang, J.-F. Liu and Y.-G. Yin, *J. Chromatogr. A*, 2011, **1218**, 6705–6711.
43 U. E. Bollmann, A. Möller, Z. Xie, R. Ebinghaus and J. W. Einax, *Water Res.*, 2012, **46**, 531–538.
44 E. Martínez-Carballo, C. González-Barreiro, A. Sitka, S. Scharf and O. Gans, *Sci. Total Environ.*, 2007, **388**, 290–299.
45 M. Venier, A. Dove, K. Romanak, S. Backus and R. Hites, *Environ. Sci. Technol.*, 2014, **48**, 9563–9572.
46 J. Gustavsson, K. Wiberg, E. Ribeli, M. A. Nguyen, S. Josefsson and L. Ahrens, *Sci. Total Environ.*, 2018, **625**, 1046–1055.
47 Z. Zhang, H. Shao, M. Wu, J. Zhang, D. Li, J. Li, H. Wang, W. Shi and G. Xu, *Arch. Environ. Contam. Toxicol.*, 2019, **77**, 115–126.
48 Y. Chen, Q. Zhang, T. Luo, L. Xing and H. Xu, *Chemosphere*, 2019, **231**, 41–50.
49 M. J. He, J. F. Lu, J. Y. Ma, H. Wang and X. F. Du, *Environ. Pollut.*, 2018, **237**, 143–153.
50 A. Marklund, B. Andersson and P. Haglund, *Environ. Sci. Technol.*, 2005, **39**, 3555–3562.
51 W. Li, Y. Wang and K. Kannan, *Environ. Int.*, 2019, **131**, 105054.
52 R. Sühring, H. Wolschke, M. L. Diamond, L. M. Jantunen and M. Scheringer, *Environ. Sci. Technol.*, 2016, **50**, 6644–6651.
53 Statistics Canada, *Population and Dwelling Count Highlight Tables*, https://www12.statcan.gc.ca/census-recensement/2016/dp-pd/hlt-fst/pd-pl/Table.cfm?Lang=Eng&T=307&S=3&O=D#details-panel2, (accessed February 2021).
54 D. Cao, J. Guo, Y. Wang, Z. Li, K. Liang, M. B. Corcoran, S. Hosseini, S. M. C. Bonina, K. J. Rockne, N. C. Sturchio, J. P. Giesy, J. Liu, A. Li and G. Jiang, *Environ. Sci. Technol.*, 2017, **51**, 1441–1449.
55 X. Wang, L. Zhu, W. Zhong and L. Yang, *J. Hazard. Mater.*, 2018, **360**, 43–50.
56 L. Pang, J. Liu, Y. Yin and M. Shen, *Environ. Toxicol. Chem.*, 2013, **32**, 2755–2761.
57 A. Sabljic, *Environ. Sci. Technol.*, 1987, **21**, 358–366.
58 E. Mullins, R. Oldland, Y. A. Liu, S. Wang, S. I. Sandler, C.-C. Chen, M. Zwolak and K. C. Seavey, *Ind. Eng. Chem. Res.*, 2006, **45**, 4389–4415.
59 A. Klamt, *J. Phys. Chem.*, 1995, **99**, 2224–2235.
60 J. Cristale, A. Álvarez-Martín, S. Rodríguez-Cruz, M. J. Sánchez-Martín and S. Lacorte, *Environ. Sci. Pollut. Res.*, 2017, **24**, 27870–27878.
61 F. A. P. C. Gobas and L. G. Maclean, *Environ. Sci. Technol.*, 2003, **37**, 735–741.
62 L. Wang, Q. Kang, Y. Jia, X. Li and J. Hu, *Environ. Sci. Technol.*, 2021, **55**, 2482–2490.
63 L. Ye, W. Meng, J. Huang, J. Li and G. Su, *Environ. Sci. Technol.*, 2021, **55**, 5836–5847.